IET Microwaves, Antennas & Propagation

Research Article

IET Journals
The Institution of Engineering and Technology

Rapid simulation-driven design of miniaturised dual-band microwave couplers by means of adaptive response scaling

ISSN 1751-8725
Received on 19th February 2016
Revised on 29th April 2016
Accepted on 17th May 2016
doi: 10.1049/iet-map.2016.0136
www.ietdl.org

Slawomir Koziel[1,2], *Adrian Bekasiewicz*[1,2] ✉

[1]*Engineering Optimization and Modeling Center, School of Science and Engineering, Reykjavík University, Menntavegur 1, 101 Reykjavík, Iceland*
[2]*Faculty of Electronics, Telecommunications and Informatics, Gdansk University of Technology, 80-233 Gdansk, Poland*
✉ *E-mail: bekasiewicz@ru.is*

Abstract: One of the major challenges in the design of compact microwave structures is the necessity of simultaneous handling of several objectives and the fact that expensive electromagnetic (EM) analysis is required for their reliable evaluation. Design of multi-band circuits where performance requirements are to be satisfied for several frequencies at the same time is even more difficult. In this work, a computationally efficient design of dual-band microstrip couplers is demonstrated by means of an adaptive response scaling (ARS) technique. ARS is a surrogate-assisted method that exploits a fast surrogate of the high-fidelity EM-simulation model of the coupler at hand constructed from its corrected equivalent circuit. ARS identifies nonlinear frequency and amplitude response scaling that accommodates the misalignment between the low- and high-fidelity models. Due to exploiting the knowledge embedded in the low-fidelity model ARS surrogate exhibits excellent generalisation capability. It is demonstrated here by optimisation of a dual-band microstrip coupler with enhanced bandwidth, working at 1 GHz and 2 GHz frequencies. The optimised design has been obtained at the cost of just a few high-fidelity EM simulations of the structure. Numerical comparisons indicate superiority of ARS over competitive surrogate-assisted techniques. Experimental validation is also provided.

1 Introduction

There are three fundamental difficulties in design optimisation of compact microwave structures. The first is the necessity of simultaneous handling of several objectives (such as matching, power split, port isolation, in case of coupler structures [1]). The second is a potentially large number of geometry parameters that need to be adjusted [2]. This gives rise from complex circuit topologies, e.g. being a result of replacing conventional transmission lines (TLs) by slow-wave compact cells (typical cell is described by four to six parameters against two for a TL) [3–5]. Finally, reliable performance evaluation of miniaturised circuits requires full-wave electromagnetic (EM) analysis [1, 2, 6], which is a result of EM cross-coupling effects that are present in highly compressed layouts. These effects, if strong, cannot be adequately represented at the level of equivalent circuit models; therefore, EM-driven design closure is mandatory for compact structures. On the other hand, increased dimensionality of the design space as well as high cost of the structure analysis does not allow for utilisation of conventional numerical optimisation algorithms [1, 29] for geometry parameter adjustment due to prohibitive computational cost they incur. Consequently, majority of designs reported in the literature (e.g. [4, 5, 7, 8]) are obtained by means of interactive approaches such as parameter sweeps. Clearly, such methods are very laborious, involve considerable human supervision, and are unable to identify truly optimum circuit dimensions.

There have been several techniques proposed over the last two decades or so to speed up EM-simulation-driven design. Majority of these methods rely on a surrogate-based optimisation (SBO) paradigm [9, 10, 29]. According to SBO, direct optimisation of an expensive computational model is replaced by iterative construction and re-optimisation of its cheaper surrogate. In microwave engineering, the most popular SBO algorithm are those involving so-called physics-based surrogates, i.e. constructed from an underlying low-fidelity model (e.g. equivalent circuit). The popular approaches include different versions of space mapping (SM), e.g. [9, 29], response correction techniques [10], feature-based optimisation [1, 11], artificial neural networks [12, 13], as well as simulation-based tuning and tuning SM [14, 15]. On the other hand, availability (although still limited) of cheap adjoint sensitivities permitted computationally feasible gradient-based optimisation, also in connection with SBO [16, 17].

Despite their considerable potential, surrogate-assisted techniques have not yet been widely accepted in microwave engineering community. Seemingly, the most important bottleneck (particularly pertinent to physics-based surrogates [6]) is that successful application of SBO may not be straightforward without certain working knowledge of numerical optimisation. Moreover, because most of SBO methods are derivative-free, they are not globally convergent [18], whereas existing convergence results (e.g. [19, 20]) are based on stringent assumptions upon low- and high-fidelity model correlations that are difficult to be verified beforehand [18]. Many SBO techniques require a rather careful implementation and problem specific knowledge. Furthermore, selection of an appropriate surrogate model setup (especially important for SM algorithms) is not always trivial [29]. Other methods such as simulation-based tuning tend to be more robust but limited in terms of possible range of applications and software requirements. In case of shape-preserving response prediction (SPRP) [10], specific assumptions concerning the shape of the system response have to be satisfied for the method to work properly.

The purpose of this work is to demonstrate a simple yet robust approach to design optimisation of compact microwave structures. The adaptive response scaling (ARS) technique proposed here is founded on tracking the changes of the underlying low-fidelity model (e.g. an equivalent circuit) that are a result of surrogate model optimisation. The response change tracking is realised through non-linear spline-based scaling of both the frequency sweep applied to the low-fidelity model and the response level. The frequency scaling is also conducted to establish relationships between the low- and high-fidelity models. A composition of the

aforementioned scaling functions permits prediction of the high-fidelity model response at a design of interest. ARS does not make any assumptions concerning the shape of the response being handled. Therefore it is generic and applicable to a wide class of structures. In this work we consider design closure of a miniaturised wideband dual-band microstrip rat-race coupler (RRC). The presented results indicate that ARS outperforms several benchmark SBO methods including several variations of SM algorithms.

2 Optimisation using surrogate models

To make the paper more self-contained and accessible for the readers with limited experience in surrogate-assisted optimisation, in this section, a brief introduction to SBO is provided, including explanation of basic concepts and properties. Subsequently, an exposition of ARS technique is given in Section 3.

The design optimisation problem to be solved can be formulated as

$$\boldsymbol{x}^* = \arg\min_{\boldsymbol{x}} U(\boldsymbol{R}_\mathrm{f}(\boldsymbol{x})) \tag{1}$$

where $\boldsymbol{R}_\mathrm{f}(\boldsymbol{x})$ is a response of the EM-simulated (high-fidelity) model of a device under design (typically, S-parameters against frequency), $\boldsymbol{x}$ is a vector of adjustable (geometry) parameters, and U encodes given design specifications; $\boldsymbol{x}^*$ is the optimum design to be found. A common situation is that the high-fidelity model is computationally expensive so that direct solving of (1) is impractical or even prohibitive because it may involve a large number of EM simulations.

In SBO [29], direct solving of (1) is replaced by an iterative procedure

$$\boldsymbol{x}^{(i+1)} = \arg\min_{\boldsymbol{x}} U(\boldsymbol{R}_\mathrm{s}^{(i)}(\boldsymbol{x})) \tag{2}$$

where $\boldsymbol{x}^{(i)}$, $i = 0, 1, \ldots$, is a sequence of approximations to $\boldsymbol{x}^*$, and $\boldsymbol{R}_\mathrm{s}^{(i)}$ is a surrogate model at iteration i. The surrogate is a fast representation of $\boldsymbol{R}_\mathrm{f}$ constructed using the low-fidelity model $\boldsymbol{R}_\mathrm{c}(\boldsymbol{x})$, e.g. an equivalent circuit.

Although there are numerous SBO algorithms developed over the years and available, majority of them share the same principle of iterative enhancement and optimisation of the surrogate. The primary difference between various SBO algorithms is in the way of constructing the surrogate model. Here, we focus on physics-based methods; however, it should be mentioned that SBO methods with data-driven surrogates (e.g. involving kriging interpolation with sequential sampling [21, 22]) is an important class of techniques, popular in many areas such as structural or aerospace engineering [23, 24].

Low-fidelity model corrections can be applied at the level of the model domain (e.g. input SM [9]), additional (preassigned) parameters of the model (e.g. implicit SM [9]) or by correcting the model response (e.g. output SM [9], ARC [25], SPRP [10]). The simplest response correction method is output SM where $\boldsymbol{R}_\mathrm{s}(\boldsymbol{x}) = \boldsymbol{R}_\mathrm{c}(\boldsymbol{x}) + \Delta$, where Δ is typically a constant vector, e.g. $\Delta = \boldsymbol{R}_\mathrm{f}(\boldsymbol{x}^{(i)}) - \boldsymbol{R}_\mathrm{c}(\boldsymbol{x}^{(i)})$. This type of correction ensures zero-order consistency between the surrogate and the high-fidelity model (i.e. $\boldsymbol{R}_\mathrm{f}(\boldsymbol{x}^{(i)}) = \boldsymbol{R}_\mathrm{s}^{(i)}(\boldsymbol{x}^{(i)})$), however, it also becomes problematic when handling highly non-linear responses [25]. Some of the problems pertinent to aforementioned response correction techniques can be overcome by the proposed ARS introduced in the next section.

3 Adaptive response scaling

In this section we give an exposition of the ARS technique. First, we introduce the ARS concept then discuss the frequency and amplitude scaling functions, and, finally describe the ARS surrogate model prediction process. Here, ARS is explained using a dual-band coupler example, utilised later in the paper for demonstration purposes.

3.1 Adaptive response scaling concept

Here, we formulate the ARS technique as a method for constructing the surrogate model for the SBO algorithm (2). As demonstrated in Section 4, ARS exhibits very good generalisation capability which translates into fast convergence of the ARS-based optimisation process.

The purpose of ARS is to construct the surrogate model that preserves zero-order consistency (i.e. ensures $\boldsymbol{R}_\mathrm{s}^{(i)}(\boldsymbol{x}^{(i)}) = \boldsymbol{R}_\mathrm{f}(\boldsymbol{x}^{(i)})$) and exhibits good generalisation. This is achieved by following both frequency and amplitude changes of the low-fidelity model responses while solving the problem (2).

The concept and operation of ARS is explained using the example compact dual-band coupler considered in Section 4. Fig. 1 shows the high- and low-fidelity model responses (here, $|S_{41}|$) at the reference design $\boldsymbol{x}^{(i)}$ and at another design $\boldsymbol{x}$. The important assumption is that the models are well correlated although their absolute misalignment may be substantial. This is observed in Fig. 1: although the discrepancy between the low- and high-fidelity model is significant (in absolute terms), the changes of the model responses are similar both in terms of the frequency shifts and the response level changes when moving from one design to another. The core of ARS is to exploit this model correlation in the process of surrogate model construction.

3.2 Frequency and amplitude scaling

The scaling process is carried out for complex S-parameter responses, separately for the respective real and imaginary parts, and, in case of dual-band couplers, separately for each band. The first step is to identify the frequency relationship between the low- and high-fidelity model at the reference design $\boldsymbol{x}^{(i)}$, i.e. the most recent design found by the algorithm (2). This relationship is described by non-linear frequency scaling function F, which is retrieved by solving

$$F^{(i)}(\omega) = \arg\min_{F} \int_{\omega_\mathrm{min}}^{\omega_\mathrm{max}} \left| r_\mathrm{f}(\boldsymbol{x}^{(i)}, \omega) - r_\mathrm{c}(\boldsymbol{x}^{(i)}, F(\omega)) \right| \mathrm{d}\omega \tag{3}$$

Here, the function F is implemented using cubic splines with 20 control points within the frequency range of interest (separately for each band of coupler operation); r_f and r_c are the high- and low-fidelity responses of interest (e.g. $\mathrm{Re}(S_{11})$, etc.); $F^{(i)}$ minimises the discrepancy between the characteristics within the frequency range of interest ω_min to ω_max. The extraction process (3) is

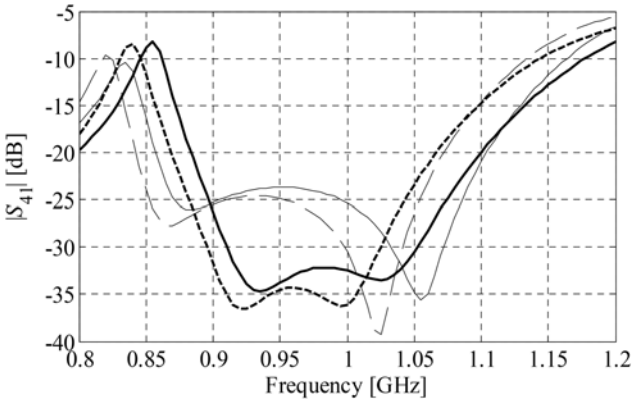

Fig. 1 *Responses of the compact dual-band microstrip coupler of Section 4: $|S_{41}|$ at a reference design $\boldsymbol{x}^{(i)}$ (—) and another design $\boldsymbol{x}$ (- - -); High- and low-fidelity models shown using thick and thin lines, respectively*

constrained to ensure monotonicity of the scaling function $F^{(i)}$ within the entire interval $[\omega_{\min}, \omega_{\max}]$.

The second step is to determine the frequency relationship between the low-fidelity model responses at the reference design $\boldsymbol{x}^{(i)}$ and at the design of interest $\boldsymbol{x}$. We have

$$F(\boldsymbol{x}, \omega) = \arg\min_{F} \int_{\omega_{\min}}^{\omega_{\max}} \left| r_c(\boldsymbol{x}, \omega) - r_c(\boldsymbol{x}^{(i)}, F(\omega)) \right| d\omega \quad (4)$$

Furthermore, the amplitude changes of the low-fidelity model are computed as (the symbol ÷ denotes component-wise division with respect to frequency)

$$A(\boldsymbol{x}, \omega) = \left[r_c(\boldsymbol{x}, \omega) + 1 \right] \div \left[r_c(\boldsymbol{x}^{(i)}, F(\boldsymbol{x}, \omega)) + 1 \right] \quad (5)$$

The shift by +1 is necessary to avoid division by zero and to avoid the scaling function getting to high values (for frequencies for which $r_c(\boldsymbol{x}^{(i)}, F(\boldsymbol{x}, \omega))$ reaches the level of −1).

It should be noted that the frequency scaling function $F^{(i)}$ is calculated only once per SBO iteration (2). On the other hand, the scaling functions F and A are calculated for each evaluation of the ARS surrogate. The cost of finding both $F^{(i)}$ and F is very low because the scaled low-fidelity model is evaluated by interpolating the known values at the original frequency sweep. In particular, that cost is negligible compared with evaluation of the high-fidelity model.

3.3 ARS model prediction

The three scaling functions described above permit prediction of the high-fidelity model response at the design of choice $\boldsymbol{x}$. The prediction procedure works as follows:

- Scale the reference high-fidelity model response $r_f(\boldsymbol{x}^{(i)}, \omega)$ in frequency using $F(\boldsymbol{x}, \omega)$ to account for the changes of the low-fidelity model when moving from the design $\boldsymbol{x}^{(i)}$ to design $\boldsymbol{x}$.
- Scale the amplitude scaling function $A(\boldsymbol{x}, \omega)$ in frequency using $F^{(i)}(\boldsymbol{x}, \omega)$ to accommodate the frequency relationships between the low- and high-fidelity model at the reference design.
- Use the scaled function A to correct the surrogate model response in amplitude.

The surrogate model is thus defined as

$$r_s(\boldsymbol{x}, \omega) = A(\boldsymbol{x}, F^{(i)}(\omega)) \circ \left[r_f(\boldsymbol{x}^{(i)}, F(\boldsymbol{x}, \omega)) + 1 \right] - 1 \quad (6)$$

where ° denotes component-wise multiplication.

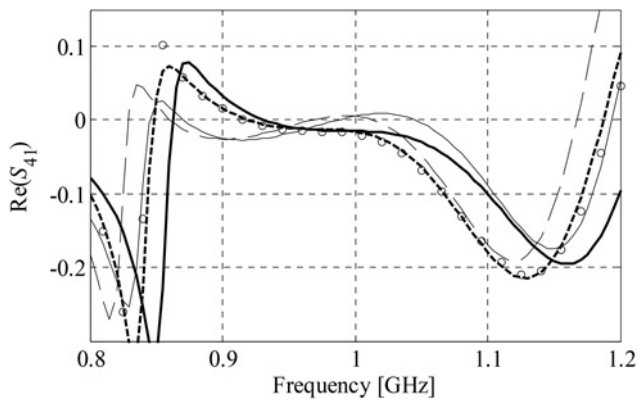

Fig. 2 *Responses of the compact dual-band microstrip coupler at $\boldsymbol{x}^{(i)}$ (—) and $\boldsymbol{x}$ (- - -) (cf. Fig. 1): $\boldsymbol{R}_f$ (thick lines) and $\boldsymbol{R}_c$ (thin lines); surrogate model response determined by (6) shown using circles*

In plain words, the prediction involves two-fold transformation of the high-fidelity model response at the reference design: first, it is scaled in frequency using the information on how the low-fidelity model changed when moving from the reference design $\boldsymbol{x}^{(i)}$ to the evaluation design $\boldsymbol{x}$; then, it is transformed in amplitude (again, using the information from the low-fidelity model change). However, the amplitude correction function is first scaled in frequency in order to account for the frequency relationships between the low- and high-fidelity models.

As mentioned before, the scaling function $F^{(i)}$ is computed only once per iteration (2). However, (4) and (5) are calculated for each evaluation of the surrogate model.

Fig. 2 shows Re(S_{41}) of the responses shown in Fig. 1 and the response of the ARS surrogate. Note that the prediction power of the model is very good. Fig. 3 shows how this translates to $|S_{41}|$ prediction. At the same time, the quality of the conventional output SM prediction is much worse as it does not account for model response changes in frequency.

4 Case study: dual-band compact microstrip rat-race coupler

In this section, the operation and performance of the ARS technique is demonstrated using compact dual-band microstrip RRC. Simulation results are validated through measurements of the fabricated coupler prototype.

4.1 Coupler structure

Consider a microstrip dual-band equal-power split RRC with enhanced operational bandwidth shown in Fig. 4. The structure is based on the conventional dual-band design of [26]. The circuit consists of six transmission line sections with stepped impedance stubs. In this work, each section is folded to the interior of the coupler which allows obtaining more compact geometry. Moreover, the high-impedance sections of the coupler have been meandered as it allows for notable reduction of the coupler size (with respect to design with unfolded geometry) without significant effect on its performance characteristics. It should be noted that the miniaturised design is characterised by increased number of degrees of freedom with respect to conventional structure, so as to enable bandwidth enhancement.

The RRC is implemented on a 0.762 mm thick Taconic RF-35 dielectric substrate ($\varepsilon_r = 3.5$, $\tan\delta = 0.0018$,). The circuit is represented by an 18-parameter vector $\boldsymbol{x} = [l_1\ l_2\ l_3\ l_4\ l_5\ l_6\ l_7\ l_8\ l_9\ l_{10}\ w_1\ w_2\ w_3\ w_4\ w_5\ w_6\ w_7\ w_8\ w_9]^T$. The dependent variables are: $l_{41} = 5l_{52} + 1.5w_2 + w_3 + 0.5w_8$, $l_{42} = 2w_3 + 0.5(l_4 - l_{41}) - 2l_{52})$, l_{43} $2w_3 + 0.5(l_3 - 5w_3)$ and $l_{51} = w_4 + 0.5l_4 - 0.5w_3 + l_{52}$, whereas $l_{52} =$ 1 and $l_{53} = 30$ remain fixed. The unit for all parameters is mm.

The high-fidelity model of the coupler has been implemented in CST Microwave Studio [27]. It consists of ∼120,000 mesh cells

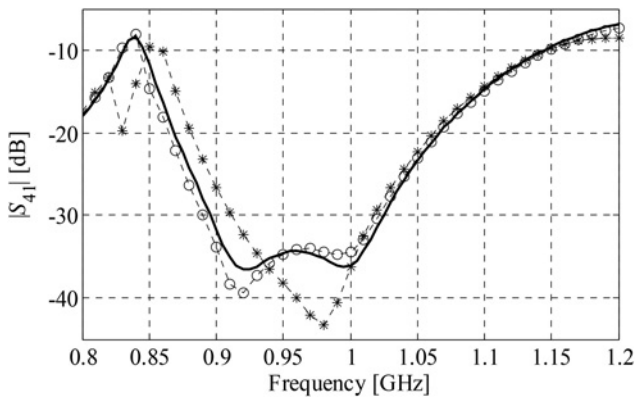

Fig. 3 *High-fidelity model response at $\boldsymbol{x}$ (thick line), and surrogate model responses obtained using ARS (o) and conventional output SM (*)*

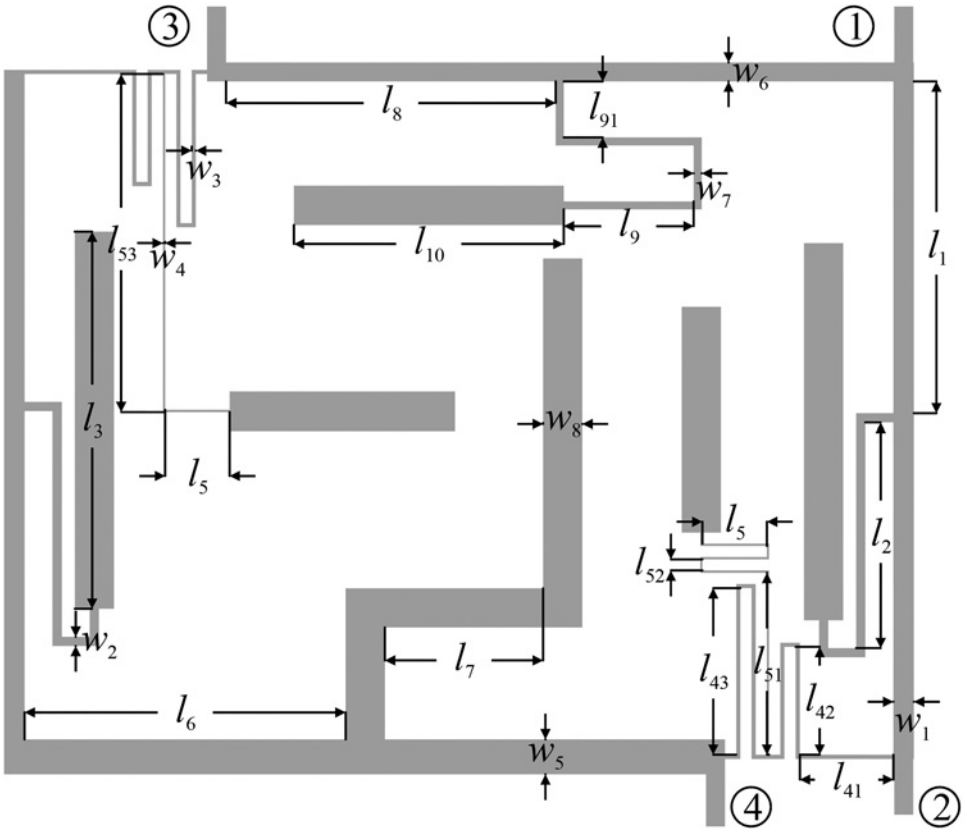

Fig. 4 *Geometry of the compact dual-band microstrip RRC with enhanced bandwidth*

and its typical simulation time on a dual Intel Xeon E5540 machine with 6 GB of RAM is 60 min. The low-fidelity model is an equivalent circuit model of the structure implemented in Agilent ADS [28].

Assumed design specifications of the miniaturised coupler structure are as follows:

- Operating frequencies: $f_1 = 1$ GHz and $f_2 = 2$ GHz.
- Equal power split.
- Bandwidth: 200 MHz for $S_{11}| \leq -18$ dB and $|S_{41}| \leq -18$ |dB.

4.2 Optimisation results and comparisons

The coupler of Fig. 4 has been optimised using the ARS algorithm. The initial design $\boldsymbol{x}^{(0)} = [29.39\ 20.72\ 33.46\ 31.91\ 5.99\ 28.45\ 14.47\ 29.66\ 11.45\ 23.34\ 1.78\ 0.79\ 0.25\ 0.20\ 2.65\ 1.74\ 0.87\ 3.98]^T$ mm is the optimum of the equivalent circuit model. The optimised design $\boldsymbol{x}^* = [29.53\ 20.36\ 32.62\ 33.94\ 7.64\ 27.92\ 13.87\ 29.76\ 12.08\ 23.33\ 1.98\ 0.83\ 0.40\ 0.21\ 3.31\ 1.42\ 0.20\ 3.64]^T$ mm has been obtained after five iterations of ARS. Note that the coupler response at the initial design exhibits considerable power split error (around 1.5 dB) at the upper operating frequency as well as considerable violation of the bandwidth requirements at both operating frequencies (see Fig. 5a).

The optimised structure features much better characteristics: the power split error is <0.15 dB at 1 GHz and <0.3 dB at 2 GHz; moreover, the maximum level of in-band matching and isolation characteristics is about −19 dB which satisfies requirements (Fig. 5b).

ARS has been compared with several variations of the SM algorithm. For fair comparison, each algorithm has been executed in an unattended manner. The results gathered in Table 1 indicate that ARS outperforms SM both with respect to the computational complexity and reliability. Except ARS, the only technique that converged was implicit SM with 14 preassigned parameters. Both, a seven parameter realisation of implicit SM and a combination of frequency and output SM algorithms were terminated due to divergence.

Table 1 Optimisation cost: ARS against benchmark methods

Optimisation algorithm	Design optimisation cost	
	Number of EM simulations	Total cost[a]
ARS (this work)	6	6.4
implicit SM[b]	13[d]	16.3
implicit SM[c]	9	12.6
frequency + output SM	3[d]	3

[a]Cost including low-fidelity model evaluations, expressed in terms of the equivalent number of EM filter simulations
[b]Seven implicit parameters related to substrate permittivity
[c]14 implicit parameters related to substrate height and permittivity
[d]Algorithm terminated due to divergence

4.3 Experimental validation

The optimised RRC design has been fabricated and measured. Photograph of the prototype is shown in Fig. 6, whereas comparison of its responses in terms of *S*-parameters and phase shift between Ports 2 and 3 is provided in Fig. 7. The results are in a very good agreement. Nonetheless, the measured power split error for the frequency f_1 is slightly worse than the simulated one. The measured phase difference is well aligned with the simulated one. It should be noted that for frequency f_2 measured response is even better than the simulated one (1° instead of –3° obtained for simulated design). Moreover, the losses within measured structure are slightly higher as compared with simulations. The discrepancies between the results are mostly because the EM model involved in the optimisation process lacks connectors. To some extent, misalignments are also the result of the fabrication process tolerances.

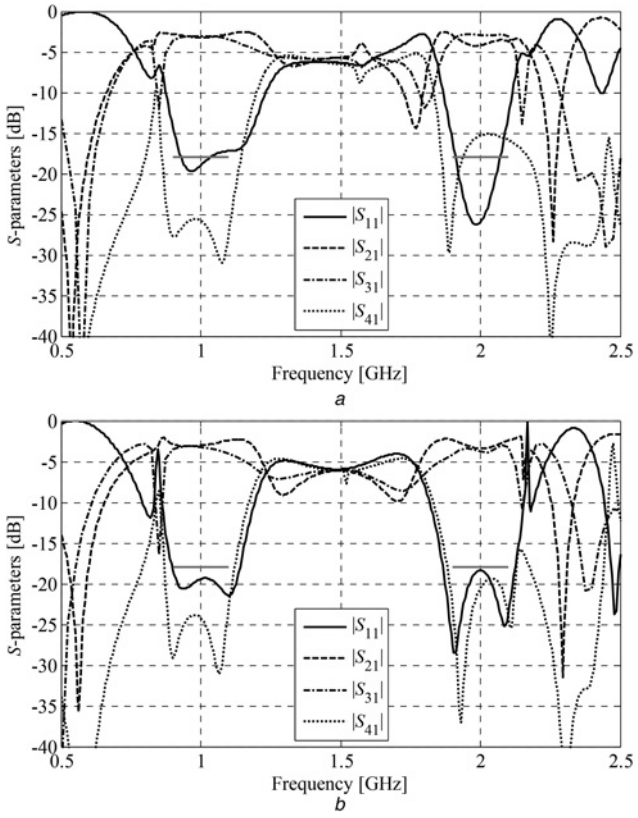

Fig. 5 *Dual-band coupler responses*

a At the initial design
b At the design obtained using ARS

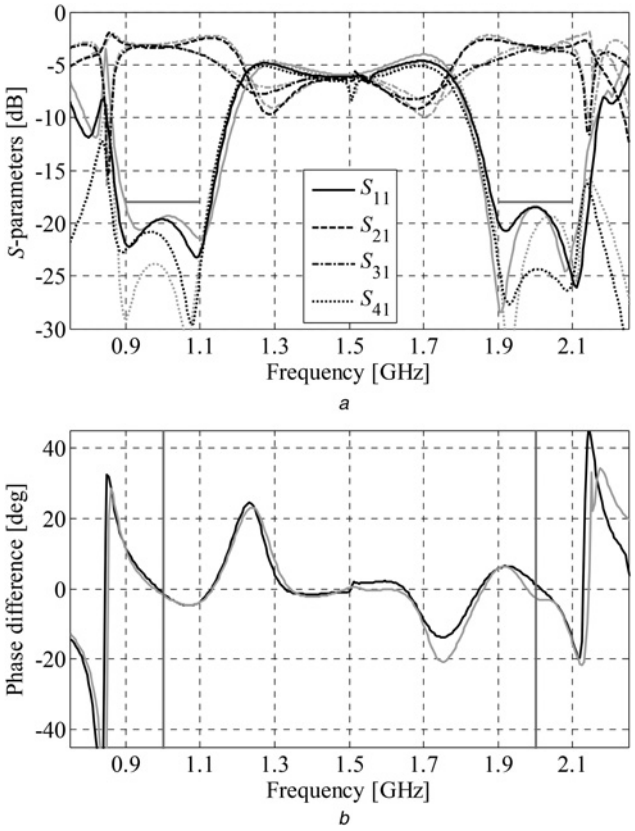

Fig. 7 *Comparison of simulated (grey) and measured (black) characteristics of the considered RRC structure*

a S-parameter response
b Phase difference between ports 2 and 3

A more detailed comparison of performance data between simulations and measurements is provided in Table 2. For the measured responses of the coupler, the bandwidth BW_1, defined as the frequency range where both return loss $|S_{11}|$ and isolation $|S_{41}|$ are below –18 dB level, is 16.7 and 16% for f_1 and f_2, respectively. The relative bandwidths have been calculated with respect to 1.5 GHz frequency. Moreover, the measured bandwidth

Table 2 Simulated against measured responses of considered RRC coupler

	Simulation		Measurement	
	f_1	f_2	f_1	f_2
S_{11} [dB]	–19.37	–18.39	–19.65	–18.50
S_{21} [dB]	–3.01	–3.40	–3.37	–3.27
S_{31} [dB]	–3.19	–3.73	–3.25	–3.51
S_{41} [dB]	–24.21	–20.54	–21.43	–24.38
BW_1 [GHz]	0.90–1.12	1.89–2.12	0.88–1.13	1.88–2.12
BW_2 [GHz]	0.91–1.02	1.95–2.01	0.90–1.04	1.98–2.07
BW_1 [%]	22	11.5	25	12
BW_2 [%]	11	3	14	4.5
$\angle(S_{21} - S_{31})$ [°]	–1.76	–2.69	–1.46	1.03

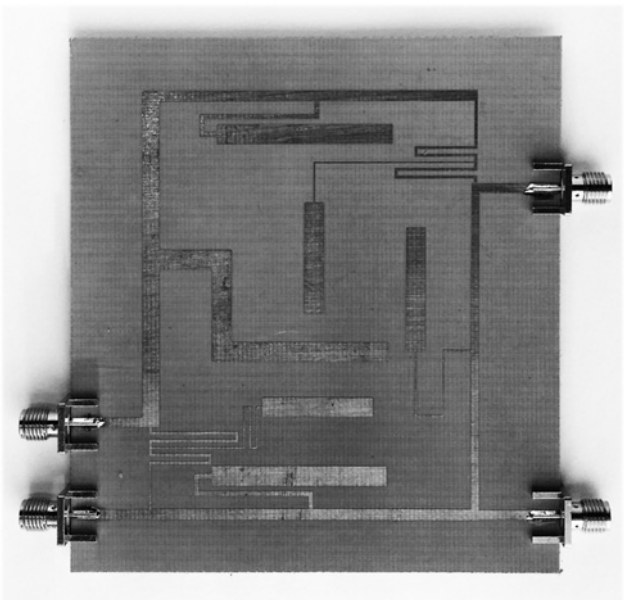

Fig. 6 *Photograph of the fabricated prototype of the optimised dual-band coupler*

BW_2, defined as the frequency range for which $| |S_{21}| - |S_{31}| | \leq 0.3$ dB, is 9.3% for 1 GHz frequency and 6.7% for 2 GHz frequency. For the simulated response, BW_1 is 14.7 and 15.3% for f_1 and f_2 frequencies, whereas BW_2 is 7 and 4%, respectively. It should be noted that the percentage-expressed bandwidth has been calculated for the frequencies f_1 and f_2, respectively. At the same time, the measured phase difference between Ports 2 and 3 (see Fig. 4) is –1.5° and 1.0° for 1 and 2 GHz frequencies, respectively, whereas values obtained from simulation are –1.8° and –2.7° for f_1 and f_2.

5 Conclusion

In this work, cost-efficient design optimisation of compact wideband dual-band microstrip couplers has been demonstrated using the ARS technique. By exploring correlations between the equivalent circuit

and the EM simulation model of the structure, ARS permits reliable handling of highly non-linear coupler responses and controlling multiple design goals even though the absolute model misalignment is significant. Model correlations are represented by appropriately extracted scaling function, concerning both frequency and amplitude relationships. Numerical comparisons indicate that ARS outperforms competitive surrogate-based optimisation algorithms, including several variations of SM. Validity of the proposed design optimisation method has also been confirmed experimentally with good agreement between the simulation and measured circuit characteristics.

6 Acknowledgments

The authors thank Computer Simulation Technology AG, Darmstadt, Germany, for making CST Microwave Studio available. This work was partially supported by the Icelandic Centre for Research (RANNIS) grants no. 141272051 and 163299-051 and by National Science Centre of Poland grant no. 2014/15/B/ST7/04683.

7 References

1 Koziel, S., Bekasiewicz, A.: 'Fast simulation-driven feature-based designoptimization of compact dual-band microstrip branch-line coupler', *Int. J. RF Microw. CAE*, 2015, **24**, (1), pp. 13–20
2 Jrad, A., Perrier, A.L., Bourtoutian, R., *et al.*: 'Design of an ultra compact electronically tunable microwave impedance transformer', *Electron. Lett.*, 2005, **41**, (12), pp. 707–709
3 Liu, C., Yang, T., Huang, K., *et al.*: 'Compact capacitive compensated directional coupler using planar artificial transmission lines', *Electron. Lett.*, 2011, **47**, (24), pp. 1321–1323
4 Kurgan, P., Filipcewicz, J., Kitlinski, M.: 'Development of a compact microstrip resonant cell aimed at efficient microwave component size reduction', *IET Microw., Antennas Propag.*, 2012, **6**, (12), pp. 1291–1298
5 Tseng, C.-H., Chang, C.-L.: 'A rigorous design methodology for compact planar branch-line and rat-race couplers with asymmetrical T-structures', *IEEE Trans. Microw. Theory Tech.*, 2012, **60**, (7), pp. 2085–2092
6 Kuo, T.-N., Lin, Y.-S., Wang, C.-H., *et al.*: 'A compact LTCC branch-line coupler using modified-T equivalent-circuit model for transmission line', *IEEE Microw. Wirel. Comp. Lett.*, 2006, **16**, (2), pp. 90–92
7 Salari, M.A., Manoochehri, O., Abbasiniazare, S.: 'Miniaturized microstrip ring hybrid with defected microstrip structure', *Microw. Opt. Tech. Lett.*, 2013, **55**, pp. 2245–2248
8 Zhang, C.F.: 'Planar rat-race coupler with microstrip electromagnetic bandgap element', *Microw. Opt. Tech. Lett.*, 2011, **53**, pp. 2619–2622
9 Bandler, J.W., Cheng, Q.S., Dakroury, S.A., *et al.*: 'Space mapping: the state of the art', *IEEE Trans. Microw. Theory Tech.*, 2004, **52**, (1), pp. 337–361
10 Koziel, S., Ogurtsov, S.: 'Design optimization of antennas using electromagnetic simulations and adaptive response correction technique', *IET Microw. Ant. Prop.*, 2014, **8**, (3), pp. 180–185
11 Koziel, S., Bandler, J.W.: 'Rapid yield estimation and optimization of microwave structures exploiting feature-based statistical analysis', *IEEE Trans. Microw. Theory Tech.*, 2015, **63**, (1), pp. 107–114
12 Gorissen, D., Zhang, L., Zhang, Q.J., *et al.*: 'Evolutionary neuro-space mapping technique for modeling of nonlinear microwave devices', *IEEE Trans. Microw. Theory Tech.*, 2011, **59**, (2), pp. 213–229
13 Devabhaktuni, V.K., Chattaraj, B., Yagoub, M.C.E., *et al.*: 'Advanced microwave modeling framework exploiting automatic model generation, knowledge neural networks, and space mapping', *IEEE Trans. Microw. Theory Tech.*, 2003, **51**, (7), pp. 1822–1833
14 Cheng, Q.S., Bandler, J.W., Koziel, S.: 'Tuning space mapping: the state of the art', *Int. J. RF Microw. CAE*, 2012, **22**, (6), pp. 639–651
15 Koziel, S., Meng, J., Bandler, J.W., *et al.*: 'Accelerated microwave design optimization with tuning space mapping', *IEEE Trans. Microw. Theory Tech.*, 2009, **57**, (2), pp. 383–394
16 Koziel, S., Ogurtsov, S., Bandler, J.W., *et al.*: 'Reliable space mapping optimization integrated with EM-based adjoint sensitivities', *IEEE Trans. Microw. Theory Tech.*, 2013, **61**, (10), pp. 3493–3502
17 Koziel, S., Bekasiewicz, A.: 'Fast EM-driven optimization using variable-fidelity EM models and adjoint sensitivities', *IEEE Microw. Wirel. Comp. Lett.*, 2016, **26**, (2), pp. 80–82
18 Koziel, S., Bandler, J.W., Madsen, K.: 'Quality assessment of coarse models and surrogates for space mapping optimization', *Optim. Eng.*, 2008, **9**, pp. 375–391
19 Koziel, S., Bandler, J.W., Madsen, K.: 'A space mapping framework for engineering optimization: theory and implementation', *IEEE Trans. Microw. Theory Tech.*, 2006, **54**, pp. 3721–3730
20 Madsen, K., Søndergaard, J.: 'Convergence of hybrid space mapping algorithms', *Optim. Eng.*, 2004, **5**, (2), pp. 145–156
21 Siah, E.S., Sasena, M., Volakis, J.L., *et al.*: 'Fast parameter optimization of large-scale electromagnetic objects using DIRECT with Kriging metamodeling', *IEEE Trans. Microw. Theory Tech.*, 2004, **52**, (1), pp. 276–285
22 Koziel, S., Bekasiewicz, A.: 'Fast multiobjective optimization of narrowband antennas using RSA models and design space reduction', *IEEE Antennas Wirel. Propag. Lett.*, 2015, **14**, pp. 450–453
23 Queipo, N.V., Haftka, R.T., Shyy, W., *et al.*: 'Surrogate-based analysis and optimization', *Prog. Aerosp. Sci.*, 2005, **41**, (1), p. 1–28
24 Forrester, A.I.J., Keane, A.J.: 'Recent advances in surrogate-based optimization', *Prog. Aerosp. Sci.*, 2009, **45**, pp. 50–79
25 Koziel, S., Bandler, J.W., Madsen, K.: 'Space mapping with adaptive response correction for microwave design optimization', *IEEE Trans. Microw. Theory Tech.*, 2009, **57**, (2), pp. 478–486
26 Chin, K.-S., Lin, K.-M., Wei, Y.-H., *et al.*: 'Compact dual-band branch-line and rat-race couplers with stepped-impedance-stub lines', *IEEE Trans. Microw. Theory Tech.*, 2010, **58**, (5), pp. 1213–1221
27 CST Microwave Studio, ver. 2013, CST AG, Bad Nauheimer Str. 19, D-64289 Darmstadt, Germany, 2013
28 Agilent (Keysight) ADS, ver. 2011.10, Agilent Technologies, 1400 Fountaingrove Parkway, Santa Rosa, CA 95403-1799, 2011
29 Bekasiewicz, A., Koziel, S., Pankiewicz, B.: 'Accelerated simulation-driven design optimisation of compact couplers by means of two-level space mapping', *IET Microw. Antennas Propag.*, 2015, **9**, (7), pp. 618–626